Journal of Alloys and Compounds 502 (2010) 387–391

Contents lists available at ScienceDirect

Journal of Alloys and Compounds

journal homepage: www.elsevier.com/locate/jallcom

Crystallization behavior and dielectric properties of $BaO–ZnO–SrO–CaO–Nd_2O_3–TiO_2–B_2O_3–SiO_2$ glass–ceramics

Hsing-I Hsiang[a,*], Li-Then Mei[a], Chi-Shiung Hsi[b], Wen-Chang Liao[a], Fu-Su Yen[a]

[a] Department of Resources Engineering, Particulate Materials Research Center, National Cheng Kung University, 70101 Tainan, Taiwan, ROC
[b] Department of Materials Science and Engineering, National United University, Miaoli, Taiwan, ROC

ARTICLE INFO

Article history:
Received 28 March 2010
Received in revised form 14 April 2010
Accepted 24 April 2010
Available online 4 May 2010

Keywords:
LTCC
Glass–ceramic
Sintering
Crystallization

ABSTRACT

The effects of heating rate on the crystallization and sintering behaviors of glass–ceramics ($BaO–ZnO–SrO–CaO–Nd_2O_3–TiO_2–B_2O_3–SiO_2$) were investigated in this study. The results showed that the onset of glass shrinkage occurred at around the glass transition temperature. The first crystalline phase, $Nd_2Ti_4O_{11}$ was observed at around 775–800 °C. Fully densified glass can be obtained via glass viscous flow before the occurrence of the second crystalline phase, $Nd_{0.66}TiO_3$. With increasing heating rate, the glass transition temperature and crystallization temperature both shift to higher temperature. Sintering at a higher heating rate can retard the $Nd_{0.667}TiO_3$ crystallization of the glass, and thus improves the sintering densification via glass viscous flow during the firing process. The Ba–Zn–Sr–Ca–Nd–Ti–B–Si glass–ceramics sintered at 900 °C with a heating rate of 20 °C/min exhibited a high dielectric constant of 25 and a quality factor of about 1460, which provided a promising candidate for LTCC applications.

1. Introduction

The microwave telecommunication and satellite broadcasting industries have progressed greatly through portable telephones. The dielectric components must also be miniaturized to reduce the device size. In recent years, low-temperature cofired ceramics (LTCC) have been developed to increase the volume efficiency by integrating passive components such as capacitors, resistors, and inductors [1,2].

The dielectric constants of commercial low dielectric loss LTCC materials are mostly around 4–5 and 7–9 [3–5]. However, the conventional LTCC material with low dielectric constant limits further miniaturization for microwave devices. Therefore, the development of LTCC with high dielectric constant is urgently desired for LTCC device fabrication for microwave applications. However, investigations into LTCC materials based on glass–ceramics with a high dielectric constant have rarely been reported in the literature [6,7].

This study presents the effects of heating rate on the crystallization, sintering behaviors and dielectric properties of $BaO–ZnO–SrO–CaO–Nd_2O_3–TiO_2–B_2O_3–SiO_2$ (Ba–Zn–Sr–Ca–Nd–Ti–B–Si) glass powder and a new developed LTCC material based on Ba–Zn–Sr–Ca–Nd–Ti–B–Si glass–ceramics with high dielectric constant and high Q, providing promising candidates for LTCC applications.

2. Experimental procedures

$BaO–ZnO–SrO–CaO–Nd_2O_3–TiO_2–B_2O_3–SiO_2$ (Ba–Zn–Sr–Ca–Nd–Ti–B–Si) glass with the composition 3.5 mol% CaO, 6 mol% SrO, 20 mol% BaO, 9.5 mol% Nd_2O_3, 20 mol% ZnO, 24 mol% TiO_2, 5 mol% B_2O_3, 12 mol% SiO_2 was prepared by melting powders containing appropriate amounts of reagent grade $CaCO_3$, $SrCO_3$, $BaCO_3$, Nd_2O_3, ZnO, TiO_2, H_3BO_3, and SiO_2 in a Pt crucible at 1550 °C for 6 h. The melt was rapidly quenched in distilled water, ball milled with Y-TZP balls for 12 h. The glass powder had a median size of 4.4 μm. The XRD (Siemens, D5000) analysis did not reveal any crystal phase for the glass powder.

The glass powder was pressed uniaxially at about 300 MPa to make a pellet 8 mm diameter and 2 mm in height. The samples were then sintered at temperatures in the range of 700–950 °C for 1 h. The crystallization behavior and the glass transition temperature (T_g) were determined using a differential thermal analyzer (DTA) (Netzsch STA 409C). The DTA was performed at a heating rate of 2–40 °C/min under flowing air. The thermal shrinkage behavior was measured using a thermal mechanical analyzer (TMA) (Mettler, 840) at a heating rate of 2–20 °C/min. The crystalline phase evolution was characterized using an X-ray diffractometer with a Cu Kα (Siemens, D5000). The microstructures of the sintered samples were examined using scanning electron microscopy (SEM) (Hitachi, S-4100). Dielectric properties (relative dielectric constant, Q value) were measured using an LCR meter (YHP 4291A, YHP Co., Ltd.) at 1 MHz.

3. Results and discussion

Fig. 1 shows the DTA curves of Ba–Zn–Sr–Ca–Nd–Ti–B–Si glass at different heating rates ranging from 2 °C to 40 °C/min. It is observed that the Ba–Zn–Sr–Ca–Nd–Ti–B–Si glass powder at a heating rate of 40 °C/min exhibits glass transition at around 716 °C, followed by one broadening and one sharp exothermic transformation occurring at around 826 and 932 °C, respectively, corresponding to glass crystallization. With decreasing heating rate, the glass transition

* Corresponding author. Tel.: +886 6 2757575x62821; fax: +886 6 2380421.
E-mail address: hsingi@mail.ncku.edu.tw (H.-I. Hsiang).

0925-8388/$ – see front matter © 2010 Elsevier B.V. All rights reserved.
doi:10.1016/j.jallcom.2010.04.176

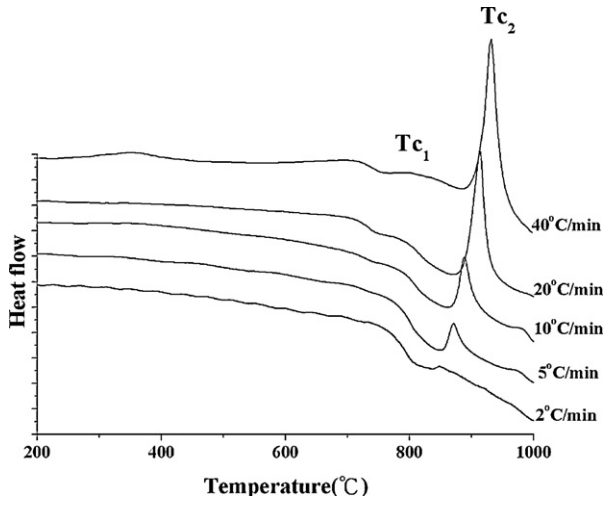

Fig. 1. DTA curves of Ba–Zn–Sr–Ca–Nd–Ti–B–Si glass at different heating rates ranging from 2 °C to 40 °C/min.

temperature and crystallization temperature both shift to lower temperature. Summary of the glass transition temperature and crystallization temperature of the Ba–Zn–Sr–Ca–Nd–Ti–B–Si glass powder measured using DTA at a different heating rate is shown in Table 1.

The XRD patterns for the Ba–Zn–Sr–Ca–Nd–Ti–B–Si glass powders sintered at various temperatures for 1 h with a heating rate of 10 °C/min are shown in Fig. 2. The glass sintered at 750 °C was still amorphous. As the sintering temperature was raised to 775 °C, the first crystalline phase, $Nd_2Ti_4O_{11}$ was observed. Therefore, the first broadening exothermic peak in the DTA curve resulted from the crystallization of $Nd_2Ti_4O_{11}$. However, the second crystalline phase, $Nd_{0.667}TiO_3$, occurred at 800 °C, determined from XRD patterns (Fig. 2), lower than the peak temperature for the sharp exothermic peak in the DTA curve. This may be because the XRD patterns were obtained for samples sintered for 1 h, which shifted the $Nd_{0.667}TiO_3$ crystallization temperature to a lower temperature compared with the DTA result. The amount of crystalline phases for the samples after sintering can be semiquantitatively determined by calculating the ratio of the integrated XRD intensities of $Nd_2Ti_4O_{11}$ (I_1) and $Nd_{0.667}TiO_3$ (I_2) to that of the XRD peak of the internal standard, rutile (I_T). Fig. 3 shows the variation in the amount of crystalline phases with the sintering temperature at different heating rates. The XRD peak intensity of the first crystalline phase, $Nd_2Ti_4O_{11}$, increased as the sintering temperature was increased from 750 to 825 °C, and then declined rapidly as the sintering temperature was raised above 825 °C. However, the second crystalline phase, $Nd_{0.667}TiO_3$, started to occur and increased with decreasing the amount of the first crystalline phase in the 825–950 °C temperature region. This implies that the formation of the $Nd_{0.667}TiO_3$ crystalline phase may result from the reaction between the crystalline phase,

Table 1
Summary of the glass transition temperature and crystallization temperature of the Ba–Zn–Sr–Ca–Nd–Ti–B–Si glass powder measured using DTA at a different heating rate.

Heating rate (°C/min)	Glass transition temperature (°C)	T_{c1} (°C)	T_{c2} (°C)
2	701	–	856
5	704	–	873
10	708	780	890
20	710	798	915
40	716	826	932

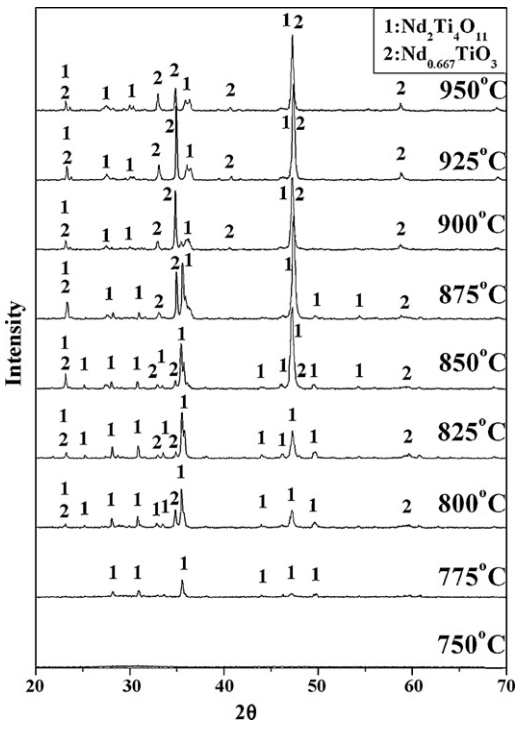

Fig. 2. XRD patterns for the Ba–Zn–Sr–Ca–Nd–Ti–B–Si glass powders sintered at various temperatures for 1 h with a heating rate of 10 °C/min.

$Nd_2Ti_4O_{11}$, and residual glass. Figs. 4 and 5 show SEM micrographs for samples sintered with different heating rates at 825 and 950 °C for 1 h, respectively. Subrounded crystals are observed at 825 °C. However, the crystal morphology becomes needle-shape at 950 °C.

Fig. 6 shows the variation in the relative densities of Ba–Zn–Sr–Ca–Nd–Ti–B–Si glass with the sintering temperature at different heating rates. The relative density increased rapidly as the sintering temperature increased from 700 to 750 °C and a relatively high relative density, above 95% (T.D.), was obtained above 750 °C for all the samples sintered at different heating rates.

Fig. 7 shows the shrinkage behaviors of the Ba–Zn–Sr–Ca–Nd–Ti–B–Si glass powder compacts at different heating rates ranging from 2 °C to 20 °C/min. For the sample at a

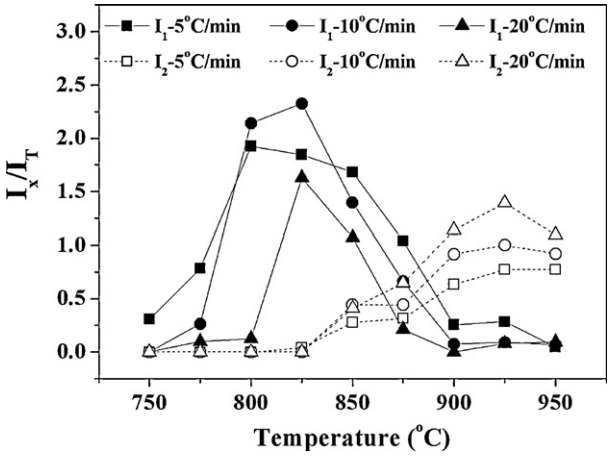

Fig. 3. Variation of the amount of crystalline phases, $Nd_2Ti_4O_{11}$ and $Nd_{0.667}TiO_3$, with the sintering temperature at different heating rates. The amount of crystalline phases for the samples sintered at various temperatures can be semiquantitatively determined by calculating the ratio of the integrated XRD intensities of $Nd_2Ti_4O_{11}$ (I_1) and $Nd_{0.667}TiO_3$ (I_2) to that of the XRD peak of the internal standard, rutile (I_T).

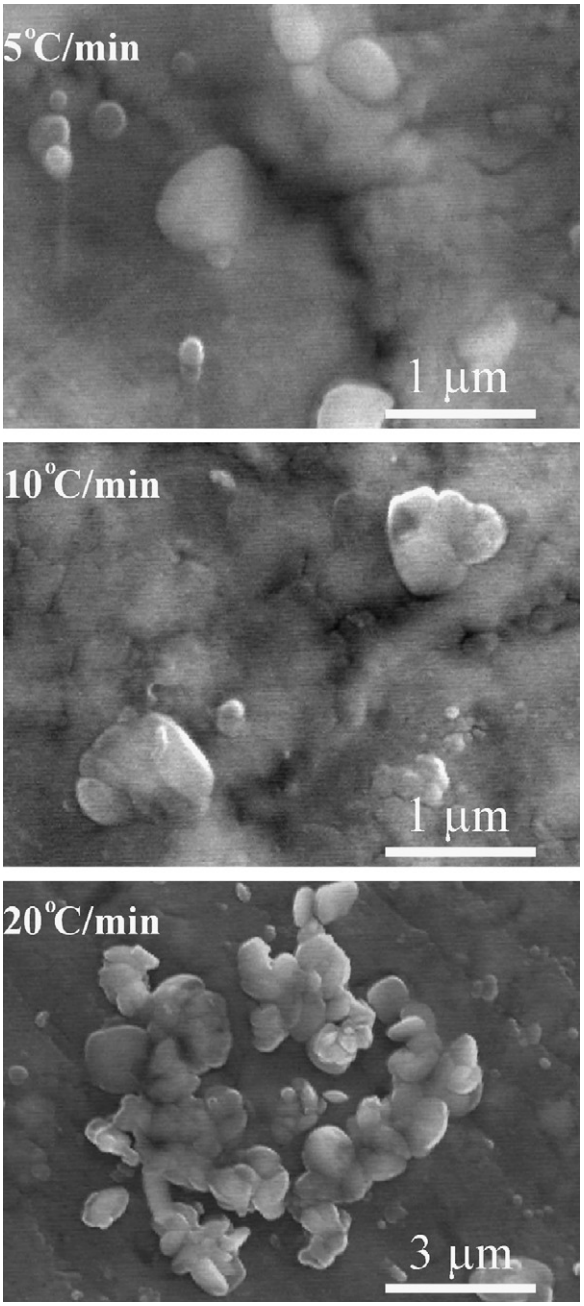

Fig. 4. SEM micrographs for samples sintered at 825 °C for 1 h with heating rates of 5, 10, and 20 °C/min.

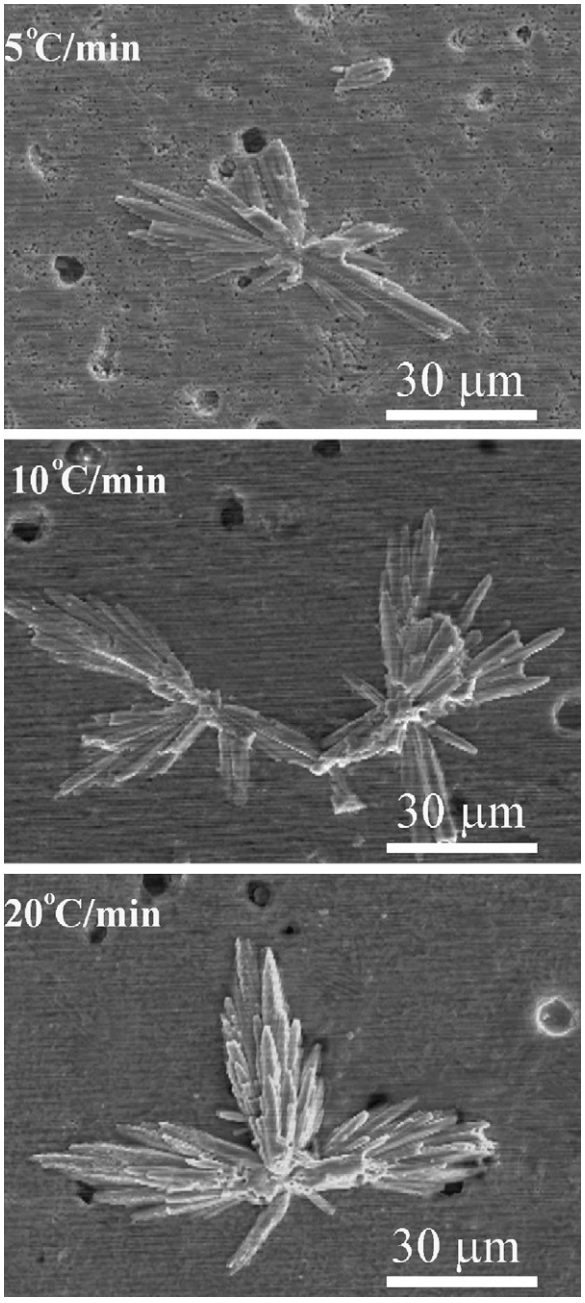

Fig. 5. SEM micrographs for samples sintered at 950 °C for 1 h with heating rates of 5, 10, and 20 °C/min.

heating rate of 2 °C/min, the onset shrinkage temperature occurred at around 720 °C, which is close to T_g, determined by DTA. The shrinkage finished at about 840 °C and the total linear shrinkage was about 15%. It is noted that the shrinkage offset temperature and total linear shrinkage increase with increasing heating rate. Fig. 8 shows the densification rate for the Ba–Zn–Sr–Ca–Nd–Ti–B–Si glass powder compact as a function of the sintering temperature at different heating rates. The first maximum shrinkage rate occurred at around 778–800 °C, which are close to the peak temperature of $Nd_2Ti_4O_{11}$ crystallization, determined by DTA. This indicates that crystallization would result in densification degradation. In addition, the secondary saddle point in the curve (Fig. 8) and the shrinkage offset temperature (Fig. 7) occurred at around 831–884 °C, which are close to the $Nd_{0.667}TiO_3$ crystalline phase temperature, determined by DTA, suggesting that full Ba–Zn–Sr–Ca–Nd–Ti–B–Si glass densification can be obtained via glass viscous flow before the $Nd_{0.667}TiO_3$ crystallization. Moreover, the densification rate and linear shrinkage for the secondary shrinkage stage (800–900 °C) increase with increasing heating rate, which are attributed to that sintering at a higher heating rate can retard the $Nd_{0.667}TiO_3$ crystallization of the glass, and thus improves the sintering densification via glass viscous flow during the firing process.

Figs. 9 and 10 show the dielectric constant and Q value of Ba–Zn–Sr–Ca–Nd–Ti–B–Si glass at different heating rate as a function of the sintering temperature, respectively. The dielectric constant value increases monotonically with increasing sintering temperature, while the Q value exhibits two maximum for samples sintered from 725 to 950 °C. The change in the dielectric properties is attributed to the variation in density and phase

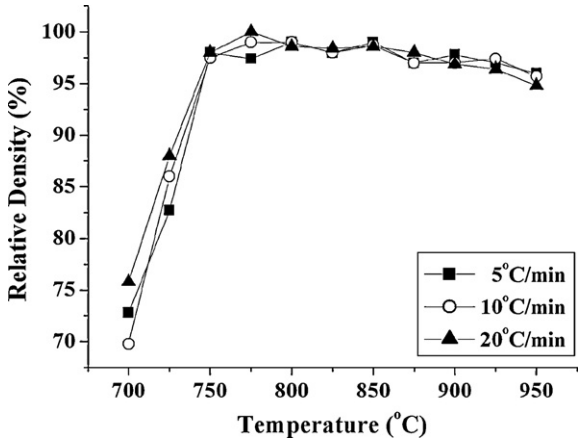

Fig. 6. Variation in the relative densities of Ba–Zn–Sr–Ca–Nd–Ti–B–Si glass with the sintering temperature at different heating rates.

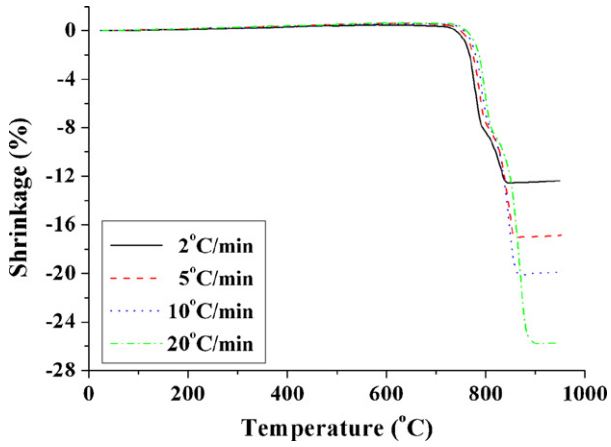

Fig. 7. Shrinkage behaviors of the Ba–Zn–Sr–Ca–Nd–Ti–B–Si glass powder compacts at different heating rates ranging from 2 °C to 20 °C/min.

constituents during sintering. In the temperature range from 725 to 825 °C, the amount of $Nd_2Ti_4O_{11}$ crystalline phase increased with increasing heating rate (Fig. 3), but the dielectric constant is independent of the heating rate, indicating that the dielectric constant of $Nd_2Ti_4O_{11}$ crystalline phase is close to that of glass. Therefore, the dielectric constant increased with increasing sintering temperature from 725 to 825 °C may be due to the increase

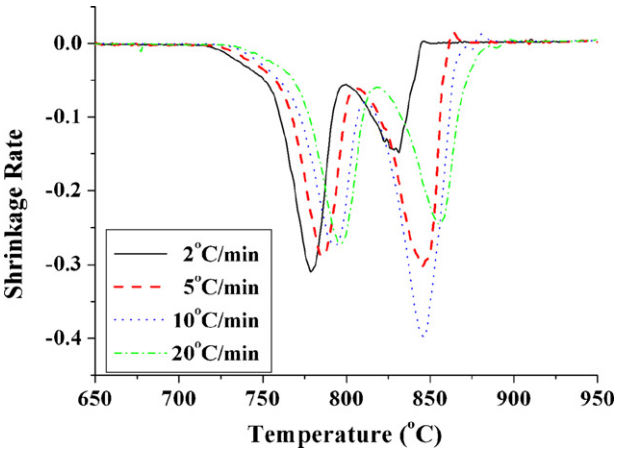

Fig. 8. Densification rate for the Ba–Zn–Sr–Ca–Nd–Ti–B–Si glass powder compact at different heating rates as a function of the sintering temperature.

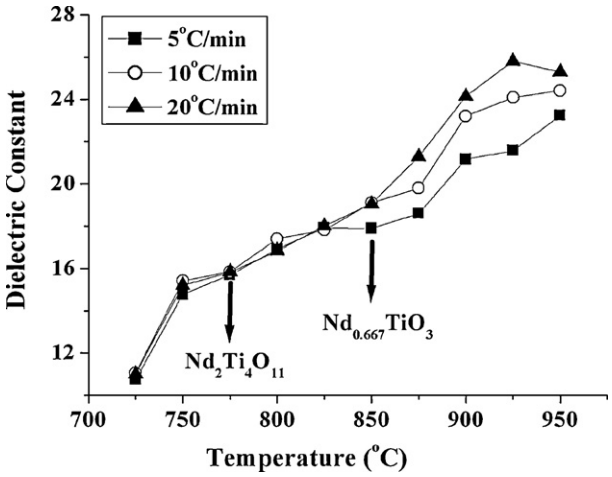

Fig. 9. Relative dielectric constant of Ba–Zn–Sr–Ca–Nd–Ti–B–Si glass at different heating rates as a function of the sintering temperature.

of relative density. In addition, as the sintering temperature was raised above 825 °C, the amount of $Nd_{0.667}TiO_3$ crystalline phase increased, thereby increasing the dielectric constant. The dielectric constant in the temperature range from 825 to 950 °C increased with increasing heating rate. This may be due to that the amount of $Nd_{0.667}TiO_3$ crystalline phase increased with increasing heating rate. The amount of crystalline phases ($Nd_2Ti_4O_{11} + Nd_{0.667}TiO_3$) for the samples sintered at various temperatures can be semiquantitatively determined by calculating the ratio of the integrated XRD intensities of $Nd_2Ti_4O_{11} + Nd_{0.667}TiO_3$ ($I_1 + I_2$) to that of the XRD peak of the internal standard, rutile (I_T). Fig. 11 shows the total amount of crystalline phases ($Nd_2Ti_4O_{11} + Nd_{0.667}TiO_3$, $I_1 + I_2$), at different heating rates as a function of sintering temperature. Note that the trend in the variation of the amount of crystalline phases with sintering temperature is similar to the quality factor (Fig. 10). It is well known that the quality factor is primarily dependent on the network structure of the remnant glass phase and the quality factor decreases with the increase in the amount of residual glass [8]. The residual glass decreases with the increase in the total amount of crystalline phases. As shown in Fig. 10, lower residual glass was observed for the samples sintered at 800 and 925 °C and at a higher heating rate (20 °C/min) in the temperature range from 900 to 950 °C, which exhibited higher quality factors. The dielectric properties of the Ba–Zn–Sr–Ca–Nd–Ti–B–Si glass–ceramics sintered at 900 °C with a heating rate of 20 °C/min show a high dielectric con-

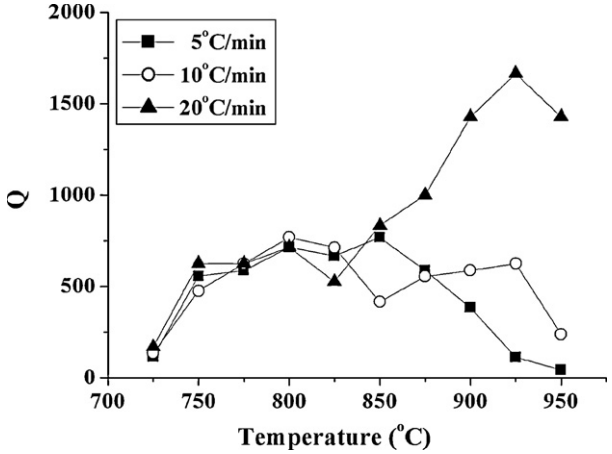

Fig. 10. Q value of Ba–Zn–Sr–Ca–Nd–Ti–B–Si glass at different heating rates as a function of the sintering temperature.

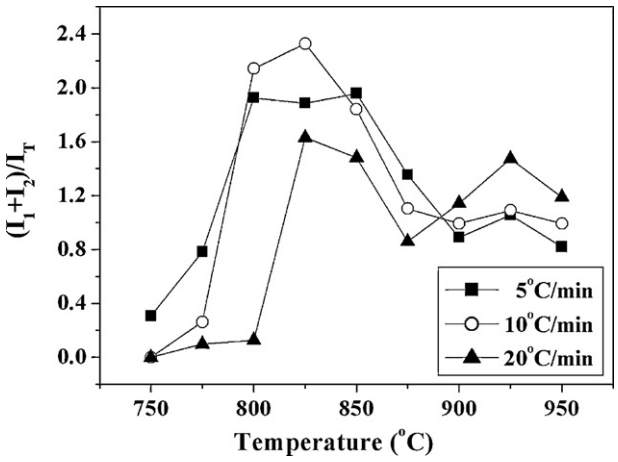

Fig. 11. Total amount of crystalline phases ($Nd_2Ti_4O_{11}$ + $Nd_{0.667}TiO_3$, $I_1 + I_2$), at different heating rates as a function of sintering temperature (I_1 and I_2: XRD peak intensities of $Nd_2Ti_4O_{11}$ and $Nd_{0.667}TiO_3$, respectively; I_T: XRD peak intensity of the internal standard, rutile).

stant of 25 and a quality factor of about 1460, which provides a promising candidate for LTCC applications.

4. Conclusions

The Ba–Zn–Sr–Ca–Nd–Ti–B–Si glass started to shrink at around the glass transition temperature, and the first crystalline phase, $Nd_2Ti_4O_{11}$ was observed at around 775–800 °C. The full densification of Ba–Zn–Sr–Ca–Nd–Ti–B–Si glass can be obtained via glass viscous flow before the occurrence of second crystalline phase, $Nd_{0.66}TiO_3$. The dielectric properties of the Ba–Zn–Sr–Ca–Nd–Ti–B–Si glass–ceramics depend on the total amount of crystalline phases. The dielectric constant and quality factor increased with the increase in the amount of crystalline phases. The dielectric constant and Q value in the temperature range from 825 to 950 °C increased with increasing heating rate. This may be due to that the amount of $Nd_{0.667}TiO_3$ crystalline phase increased with increasing heating rate. The dielectric properties of the Ba–Zn–Sr–Ca–Nd–Ti–B–Si glass–ceramics sintered at 900 °C with a heating rate of 20 °C/min show a high dielectric constant of 25 and a quality factor of about 1460, which provides a promising candidate for LTCC applications.

Acknowledgment

This work was financially sponsored by the National Science Council of the Republic of China (98-2221-E-006-077-MY3).

References

[1] A. Baker, M. Lanagan, C. Randall, E. Semouchkina, G. Semouchkin, K.Z. Rajah, R. Eitel, K.Z. Rajab, R. Mittra, S. Rhee, Int. J. Appl. Ceram. Technol. 2 (2005) 514.
[2] Y.S. Lin, C.C. Liu, K.M. Li, C.H. Chen, IEEE Trans. Micro Theory Technol. 52 (2004) 2718.
[3] C.R. Chang, J.H. Jean, J. Am. Ceram. Soc. 82 (7) (1999) 1725–1732.
[4] C.L. Lo, J.G. Duh, B.S. Chiou, W.H. Lee, J. Am. Ceram. Soc. 85 (9) (2002) 2230–2235.
[5] T. Takada, K. Kageyama, Jpn. J. Appl. Phys. 44 (9A) (2005) 6629–6635.
[6] B. Rangarajan, B. Jones, T. Shrout, M. Lanagan, J. Am. Ceram. Soc. 90 (3) (2007) 784–788.
[7] B. Rangarajan, T. Shrout, M. Lanagan, J. Am. Ceram. Soc. 92 (11) (2009) 2642–2647.
[8] G.H. Chen, X.Y. Liu, J. Mater. Sci.: Mater. Electron. 17 (2006) 877–882.